Biophysical Chemistry 149 (2010) 12–21

Contents lists available at ScienceDirect

Biophysical Chemistry

journal homepage: http://www.elsevier.com/locate/biophyschem

Natural polyphenols as inhibitors of amyloid aggregation. Molecular dynamics study of GNNQQNY heptapeptide decamer

Workalemahu M. Berhanu [a], Artëm E. Masunov [a,b,*]

[a] NanoScience Technology Center and Department of Chemistry, University of Central Florida, Orlando, FL 32826, United States
[b] Department of Physics, University of Central Florida, Orlando, FL 32826, United States

ARTICLE INFO

Article history:
Received 23 December 2009
Received in revised form 25 February 2010
Accepted 4 March 2010
Available online 18 March 2010

Keywords:
Amyloid fibril
Molecular dynamic simulation
Prion disease
β sheet
Aggregation
Oligomer
Hydrogen bond
Beta sheet inhibitor
Myricetin

ABSTRACT

Amyloid-like fibrils had been associated with many fatal diseases, and the rational design of the fibrillization inhibitors holds the great promise of finding the prevention and treatment options. The understanding of the mechanisms by which the small molecules can inhibit the aggregation plays the key role in such design. Here we present the results of MD simulations that provide the atomistic details of the process, by which the small molecules may destabilize the ordered amyloid oligomers formed by the model hexapeptide. We select a heptapeptide fragment (GNNQQNY) from Sup-35 yeast prion protein, which is capable to form both amyloid fibrils and microcrystals. Atomic-resolution structures of its crystals were reported by Eisenberg et al. (Nature 447:453, 2007). We analyze several MD trajectories describing the evolution of the decamer fragment taken from this crystal structure, both by itself and in the presence of myricetin and kaempferol (two naturally occurring polyphenols, found to be strong and weak aggregation inhibitors). While the decamer of GNNQQNY demonstrates remarkable stability of its structure after 2 ns simulation, myricetin disturbs the aggregation. The simulations show myricetin interacts with the β-sheet due to polar interactions with side chains of the peptide weakening the interstrand hydrogen bonds, wrapping the β-sheet and disaggregating the outer layer. Both backbone to backbone and side chain to side chain hydrogen bonds are lost, and the β-sheets are moving away from each other. This leads to the loss of backbone H-bonding and eventual separation of one β-strands from the outer layer. We also test several AMBER force fields and implicit solvent models for their ability to keep the decamer of GNNQQNY aggregated. The RMSDs of decamer of GNNQQNY with force field 99SB and implicit solvent models of igb2 and igb5, were maintained at less than 4 Å.

1. Introduction

Many proteins, when placed in appropriate conditions, can misfold and aggregate into a fibril agglomerates, called amyloids. These fibrils were found to have characteristic X-ray diffraction pattern and are often identified by staining with Congo red [1,2]. Amyloid-like fibrils had been associated with many fatal diseases, including Alzheimer's disease, type II diabetes mellitus, and the transmissible spongiform encephalopathies, and prion diseases [3], which affect millions of people throughout the world. The mature fibrils, and, more importantly, soluble oligomers had been recently shown to have a key role in the cytotoxic nature of amyloidogenic proteins [4]. Currently, there are no approved therapeutic agents directed against the formation of fibrillar assemblies. Over the past few years, significant research effort was made toward developing of therapeutics and chemical probes that inhibit these specific protein–protein interactions [5,6]. Apart from small molecules, a number of peptidomimetic aggregation inhibitors have been developed, based on the core fragments of amyloid peptides. Many of these inhibitors are assumed to interact with the protofibrillar and fibrillar species through formation of the main-chain β-sheet hydrogen bonds. Presumably, their inhibition mechanism is based on capping the β-sheet extension. In contrast, small molecule non-peptidic inhibitors have also been studied, including small aromatic molecules such as phenol red, polyphenols etc. These non-peptidic molecules might exhibit different interaction patterns and inhibition mechanisms compared to the peptidomimetic inhibitors. Study on the difference of the two types of inhibitors should provide more insight into the amyloid inhibition mechanisms leading to rational design of inhibitors [6]. Molecular simulations are becoming an important part of the rational design strategy. They are based on a model representing the amyloid and involve analysis of MD trajectories.

Decades of investigations of the structural properties of amyloids have established that all the fibrils have a common structural motif, called cross-β spine that consists of the β-sheets parallel to the fibril

* Corresponding author. NanoScience Technology Center, University of Central Florida, 12424 Research Pkwy, Ste 400, Orlando, FL 32826, United States. Tel.: +1 321 662 2724; fax: +1 407 882 2819.
E-mail address: amasunov@mail.ucf.edu (A.E. Masunov).

0301-4622/$ – see front matter © 2010 Elsevier B.V. All rights reserved.
doi:10.1016/j.bpc.2010.03.003

axis, with their extended protein strands perpendicular to the axis [7]. Due to the non-crystalline and insoluble nature of the amyloid fibril, it is difficult to obtain atomic-resolution structures with traditional experimental methods. However, some short peptides are capable to form both fibrils and microcrystals that are sometimes found together in solution [8]. Recently, several crystal structures of a hexa- and heptapeptides, identified as fibril-forming segments of the known pathological proteins were reported [2]. These microcrystals have similar diffraction patters to the fibrils and are capable to serve as nucleation sites for the fibril growth. These evidence indicate that atomic-resolution structures of these crystals make a good model for amyloids and can be used to investigate the mechanism of amyloid formation and disaggregation by molecular modeling methods.

One of the crystal structures determined in the work [2] was that of the heptapeptide fragment (GNNQQNY) from Sup-35 yeast prion protein. This short fragment displays many of the common characteristics as a full-length Sup-35, including cooperative kinetics of aggregation, fibril formation, and binding of the dye Congo red [8]. Molecular dynamics simulations for the pairs of β-sheets containing 3 to 50 strands of the heptapeptide GNNQQNY cut out from the crystal structure indicate that while the cross-β spine architecture is preserved, the β-sheets are twisted in the absence of the crystal packing [9]. The pair of β-sheets taken from GNNQQNY crystal structure is shown on Fig. 1. This fragment demonstrates the cross-β spine architecture with the β-sheets separated by a dry, non-hydrated interface. Each β sheet is formed by parallel strands. In addition to the classical hydrogen bonds between backbone atoms, the β sheets are stabilized by hydrogen bonds between the matching polar side chains (so-called the polar zipper). At the dry interface, the side chains of residues N2, Q4 and N6 are also tightly interdigitated with the corresponding residues of the opposing sheet (structure is known as steric zipper) [2,8].

Fragments of GNNQQNY crystal structure present an attractive target for theoretical studies of aggregation and disaggregation. A number of theoretical works explored the early aggregation behavior of the GNNQQNY sequence [10–12]. Zheng et al. [12] performed simulations of various oligomers of the original peptide and its mutants to study its stability and dynamics in the explicit solvent. Different sizes and arrangements of the aggregates were studied. The results showed that the stability of the oligomer increased dramatically with the increase in the number of strands, suggesting that the even a small nucleus can serve as a seed for the fibril formation. The

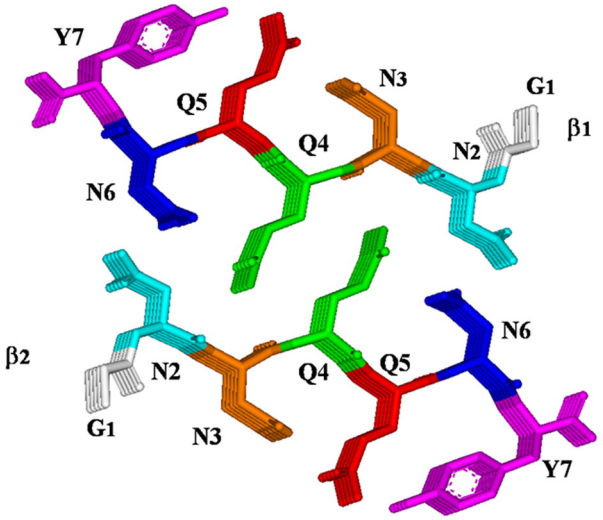

Fig. 1. The atomic presentation of the GNNQQNY oligomer; sandwich of 2 beta sheets formed by 5 heptapeptides each. Intersheet steric zipper is formed between the side chain of the residues Asn-2, Gln-4 and Asn-6 of the β1 sheet and those of the same residue of β1 sheet.

MD simulations also show that within sheet, the driving forces to associate and stabilize are interstrand backbone–backbone and side chain–side chain hydrogen bonds, whereas between sheets, shape complementary by dry polar steric zipper via the side chains of Asn-2, Gln-4, and Asn-6 holds the sheets together. Moreover, mutant simulations showed that the correct geometrical matching of the side chains via intersheet interaction plays an important role in determining the stability of oligomers. In another study Gsponer et al. [13] found that the parallel β sheet arrangement is favored over the anti-parallel one because of stacking interactions of the tyrosine rings and hydrogen bonds between amide groups. The disaggregation mechanisms of the GNNQQNY fibrils and its aggregation pathways were investigated by high-temperature molecular dynamics simulation in explicit solvent by Wang et al. [14]. Hexamer and dodecamer models, both with two parallel β-sheets separated by a dry side chain interface were adopted in their computational analysis. Landscape and kinetics analyses also indicate that the parallel β-sheets form earlier than the dry side chain contacts during aggregation.

Apart from the understanding the amyloid fibril formation, study of the small aggregates may help to understand the role of oligomers in amyloid diseases. There are several hypotheses suggesting different mechanisms for amyloid toxicity [15,16]. Some recent experimental results focus the attention on soluble oligomeric aggregates, which were shown to be more toxic than fully formed mature amyloid fibrils [17,18]. The mounting body of evidence reveals a strong correlation between the cognitive deficit in mice and the amount of soluble oligomers assembled from the monomeric constituent peptides [19–21]. Compounds that inhibit aggregation, fibrillization, and/or plaque formation may be capable to reduce this toxicity and thus display therapeutic effect. Various small molecule aggregation inhibitors have been recently discovered [16]. The well known example is Congo red, a sulfonated dye that specifically binds to amyloids and is commonly used histological dye for amyloid detection. It was reported to inhibit fibrillization and neurotoxicity of Aβ [15]. Unfortunately, this dye cannot cross the blood-brain barrier and is carcinogenic if given orally, thereby hindering its therapeutic use [15]. Natural polyphenolic compounds found in teas, berries, fruits, spices, and plants were known to have antioxidative, and anti-inflammatory activities. Recently their significant effects on fibril formation, nucleus formation/extension and disaggregation were also discovered [22–24]. In this study we focus on myricetin (Scheme 1), which was reported to be the most potent among the polyphenolic group of compounds.

There have been several theoretical attempts to study the interactions between current inhibitors and oligomers at the atomic level [21,25–27]. Using all-atom molecular dynamics simulations with explicit solvation model, Wu et al. [26] have identified and characterized two specific binding modes of Congo red molecules to protofibrils formed by GNNQQNY. Two potential inhibition mechanisms of disrupting β-sheet stacking were identified and suggested to use for the development of non-peptidic amyloid-specific inhibitors.

Convertino et al. [25] used MD with implicit solvent to investigate the influence of two planar aromatic compounds, 9,10-anthraquinone (AQ) and anthracene (AC), on the early phase of the aggregation of the Aβ heptapeptide segment H14QKLVFF20, the hydrophobic stretch that promotes the Aβ self-assembly. The simulations show that AQ interferes with β-sheet formation more than AC. In particular, AQ

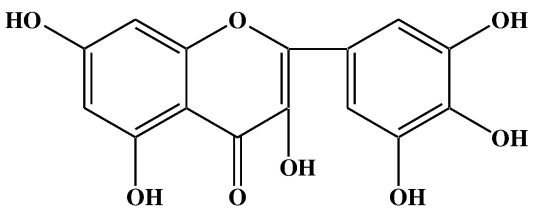

Scheme 1. Structure of myricetin.

intercalates into the β-sheet because polar interactions between the compound and the peptide backbone destabilize the interstrand hydrogen bonds, thereby favoring disorder.

Liu et al. [27] investigated the molecular mechanism of the inhibition effect of trehalose on Aβ16–22 and Aβ40 peptides with MD in explicit solvent. The simulations confirmed that Aβ16–22 aggregation is prevented by trehalose in a dose-dependent manner, and it is found that the preferential exclusion effect of trehalose is the origin of its inhibitors effects. Namely, there is preferential hydration within 3 Å of the peptide surface, and trehalose molecules cluster around the peptides at a distance of 4–5 Å. At high trehalose concentrations, the preferential exclusion of trehalose leads to three sequential effects that prevent the nucleation and elongation of Aβ16–22 oligomers. First, the secondary structures of Aβ16–22 monomers are stabilized in the turn, bend, or coil, so the β-sheet-rich structure that is prone to forming peptide oligomers is prevented. Second, the thin hydration layer and trehalose clusters can weaken hydrophobic interactions that lead to Aβ16–22 aggregation. Third, more direct and indirect H-bonds form between trehalose and Aβ16–22, which suppress the interpeptide hydrogen bonding.

Mothana et al. [28] have studied the complexes between Aβ13 and Aβ23 and three pseudo peptidic β-sheet inhibitors, as well as its homodimer. They employed MD technique called "atomic force microscopy" (AFM) to examine the dynamics of dissociation of the complexes in water. Each ligand attached to Aβ (13–23) begins dissociation by peeling back from its C-terminus, breaking interstrand H-bonds, and losing the β-sheet character. The salt bridges are the last to release, and presumably are the first to form in the reverse process of aggregation. The free energy profiles of the dissociation as a function of the separation of the centers-of-mass of all systems show plateau regions in which separation takes place with relatively little or no rise in free energy. For each system the dissociation profile does not have a maximum and reaches a flat plateau. By implication, the reverse process of assembly does not have a barrier. These plateau regions in the dissociation profile are examples of entropy–enthalpy compensation that arise naturally during the AFM-MD simulation.

In this work we focus on theoretical investigation of the dis-aggregation effect of myricetin molecule on GNNQQNY oligomers in order to understand the mechanism of this effect.

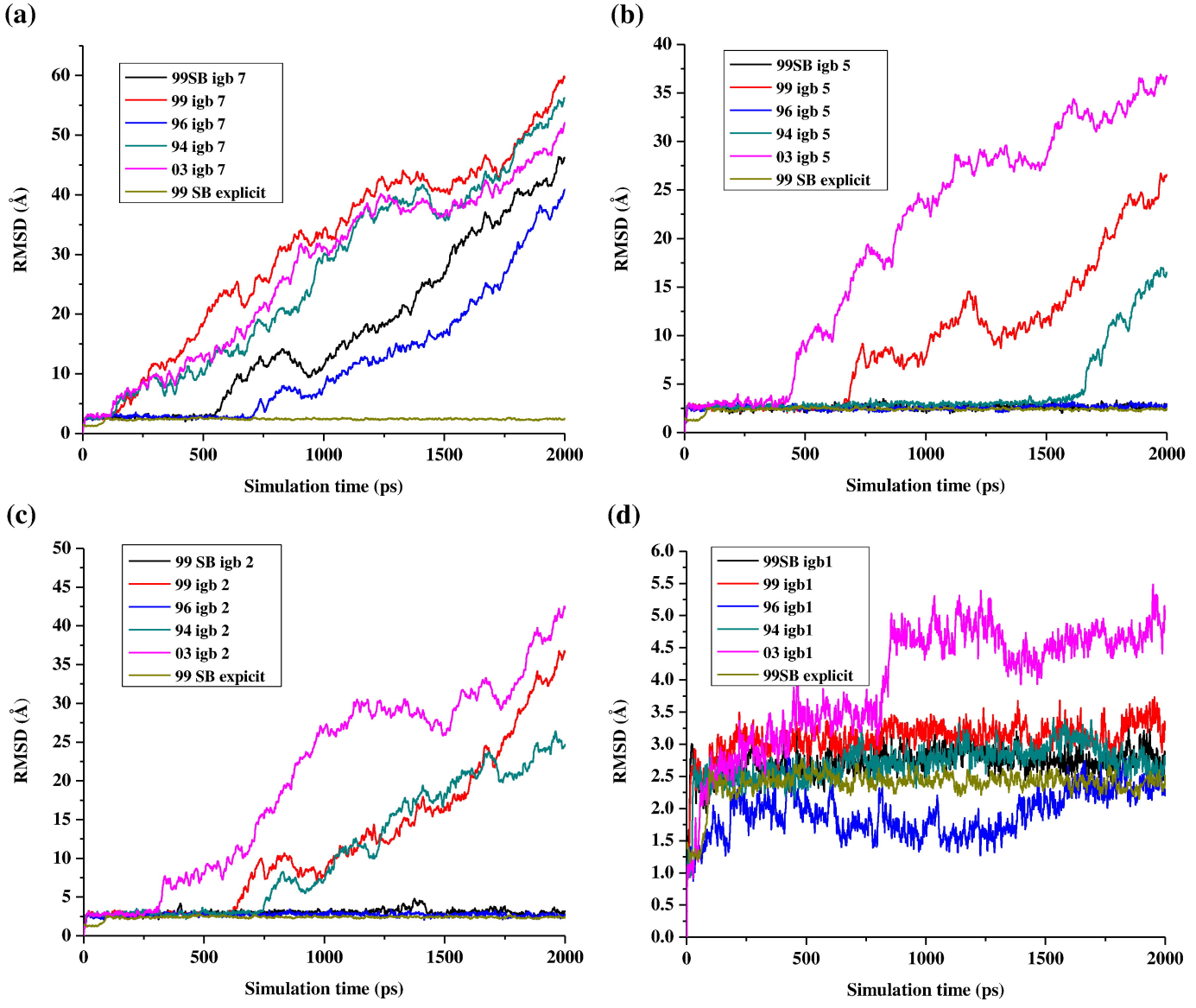

Fig. 2. Comparison of root mean square deviations (RMSD in angstrom) of MD trajectories for implicit solvent models and explicit solvent simulation (SB99 force field) (a) igb7, (b) igb5, (c) igb2 and (d) igb1.

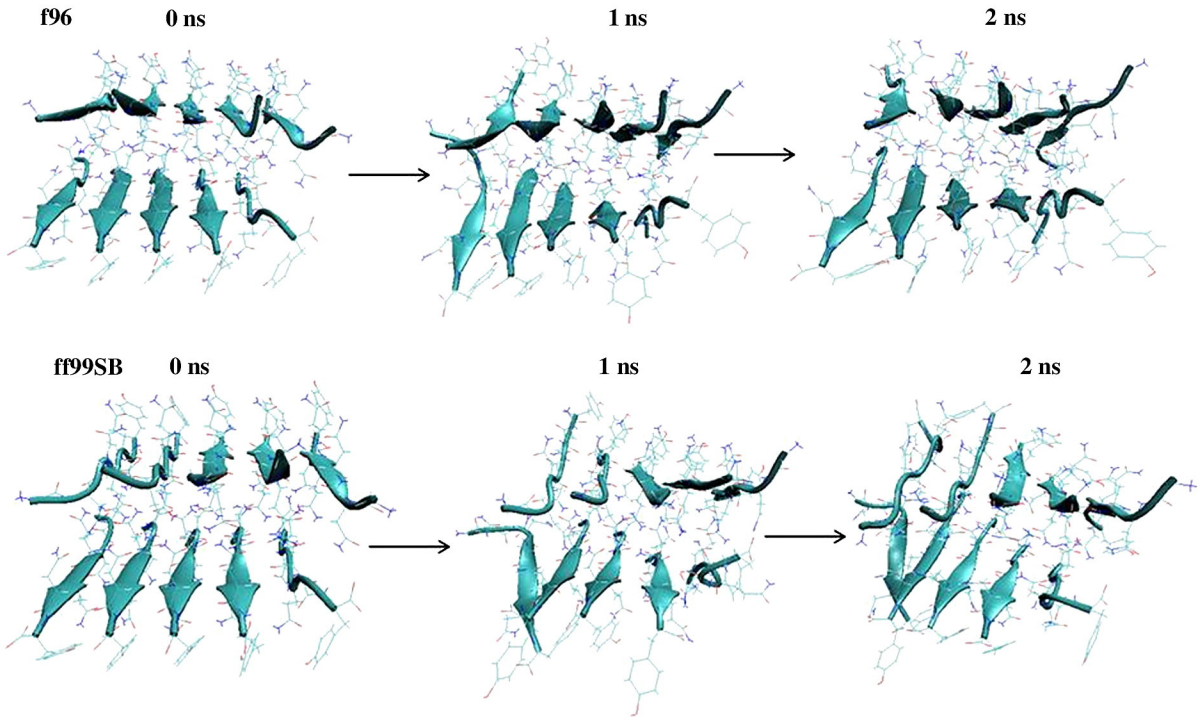

Fig. 3. Structural snapshots of GNNQQNY oligomer with igb2 implicit solvent model at 0, 1000 and 2000 ps in the simulations with ff 96 and ff99SB force fields. The figure was generated using VMD.

2. Computational details

2.1. The choice of the force fields and implicit solvent models

Conventional all-atom MD simulations of biomolecules with explicit solvent are computationally expensive and cover relatively short time scales as a result. In order to overcome this limitation, implicit solvent models are often used for simulation of large macromolecular systems and longer time scales [29–32]. In the explicit solvent approach the water is treated at atomic level, necessitating a detailed description of interactions between the solvent molecules which is not always relevant to the biomolecules of interest. In contrast, implicit models

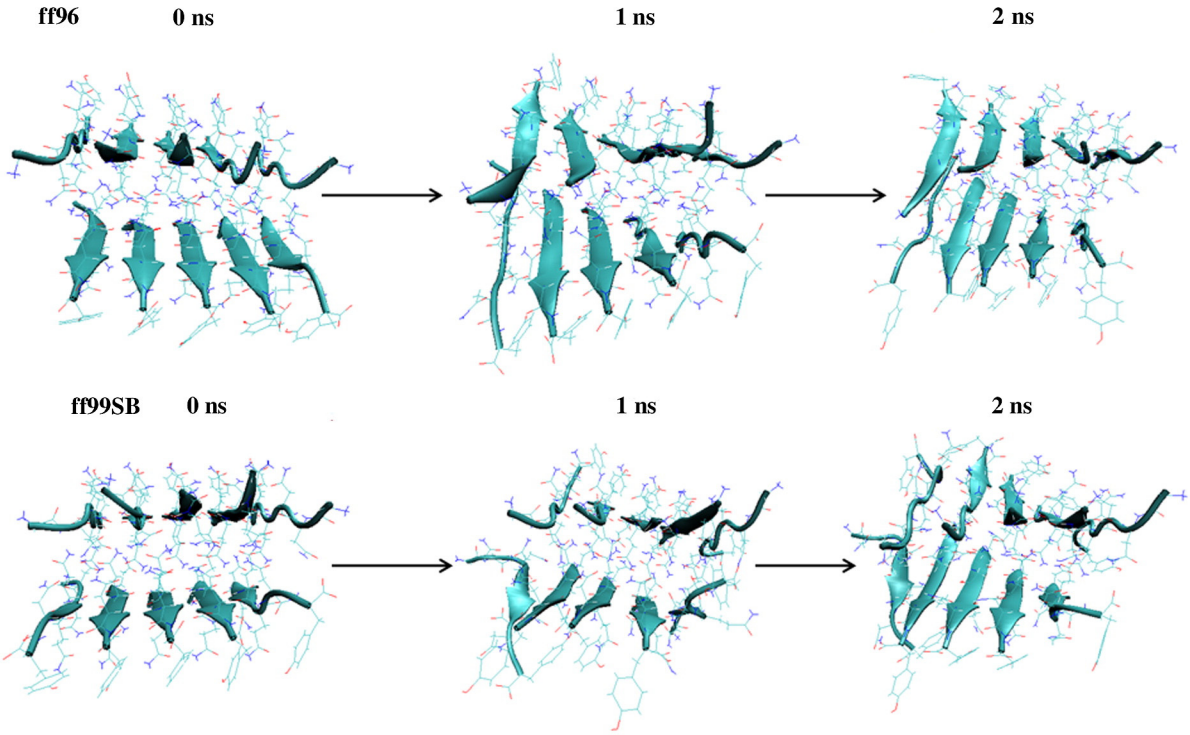

Fig. 4. Structural snapshots of GNNQQNY oligomer with igb5 implicit solvent model at 0, 1000 and 2000 ps in the simulations with ff 96 and ff99SB force fields. The figure was generated using VMD.

average out these details by considering the solvent as a dielectric continuum and are thus more computationally efficient [33]. Implicit solvent methods are designed to reproduce the solvation free energy as a function of protein composition and conformation, in mean-field term that can be added to the intra-molecular Hamiltonian for the protein. Implicit models represent the solvent as a uniform dielectric medium, neglecting the geometry and detailed bonding patterns of the solvent, such as water's hydrogen bonds. Short and long-range components of this free energy are treated separately: short-range interactions include van der Waals attractions and the formation of the protein cavity, and are typically modeled as being proportional to the solvent-accessible surface area. Implicit solvent-based methods play an increasingly important role in molecular modeling of biomolecular structure and dynamics [34]. Along with the methodological advances, implicit solvent models have enjoyed success in a range of areas, such as protein design, structure refinement, protein–protein, protein–nucleic acid, and protein–ligand interactions. They had been also used to understand protein folding and misfolding at atomistic level of details [34].

Presently there are several all atom force fields available for simulations of the proteins. Not all of them describe specific characteristics of the protein structure and properties equally well. In fact, use of some force fields may lead to biased structural distributions. Several issues remain to be solved in force field developments, such as compatibility with implicit solvent models, efficient conformational sampling and proper treatment of the backbone interactions for secondary structure propensities [35,36]. Shell et al. tested different force fields and implicit solvent models available in AMBER. They found the different combinations of force fields captured the correct secondary structures with various successes [37]. In the present study, we examine five AMBER force fields: ff96, ff94, ff99, ff99SB, and ff03. The original ff94 parameter set developed by the Kollman group [38] is one of the earlier force fields adopted by many researchers. The implicit solvent models available in AMBER are: igb1, igb2, igb5, and igb7. We test their combinations, and identify the ones that preserve the structure of the pair of β-sheets taken from GNNQQNY crystal. The best combination of force fields and implicit solvent models is then used for investigating the atomic level interaction of the oligomer with myricetin which is experimentally known to destabilize an already formed amyloid oligomer.

Assuming that common structural characteristics for all amyloid-like fibrils imply common mechanism of pathogenesis [39], we have utilized the GNNQQNY crystal structure and molecular dynamics simulations in implicit water to understand the disaggregation mechanisms of the fibrils in the presence of natural polyphenolic (myricetin) compounds.

2.2. Structure preparation

Before carrying out molecular dynamics (MD) simulations, the force parameters for myricitin were generated by GAFF utility [2] in AMBER suite. Geometry optimization and partial charges were obtained using Gaussian03 [40]. After geometry optimization at HF/6-31G* level, the partial charges were derived by fitting to the gas-phase electrostatic potential at the same theory level using the restrained electrostatic potential (RESP) method. In order to validate the force field parameters of myricetin, 2 ns simulation with the implicit solvent was performed. The bond lengths and bond angles were well maintained in the MD simulations in agreement with HF/6-31G* structure. The parameter file in AMBER format is available as Supplementary Material.

The crystal structure of the GNNQQNY had been determined by Sawaya et al. [2]. The atomic coordinates were taken from [41]. The first out of two different polymorphic forms (forms 1 and 2 with resolution of 1.8 and 2.0) was used. We selected a sandwich of two β-sheets (5 strands each), stabilized by hydrogen bonds between polar side chains (the polar zipper) (Fig. 1). The complex between the polyphenolic compound and the peptide was made using the Sirius visualization

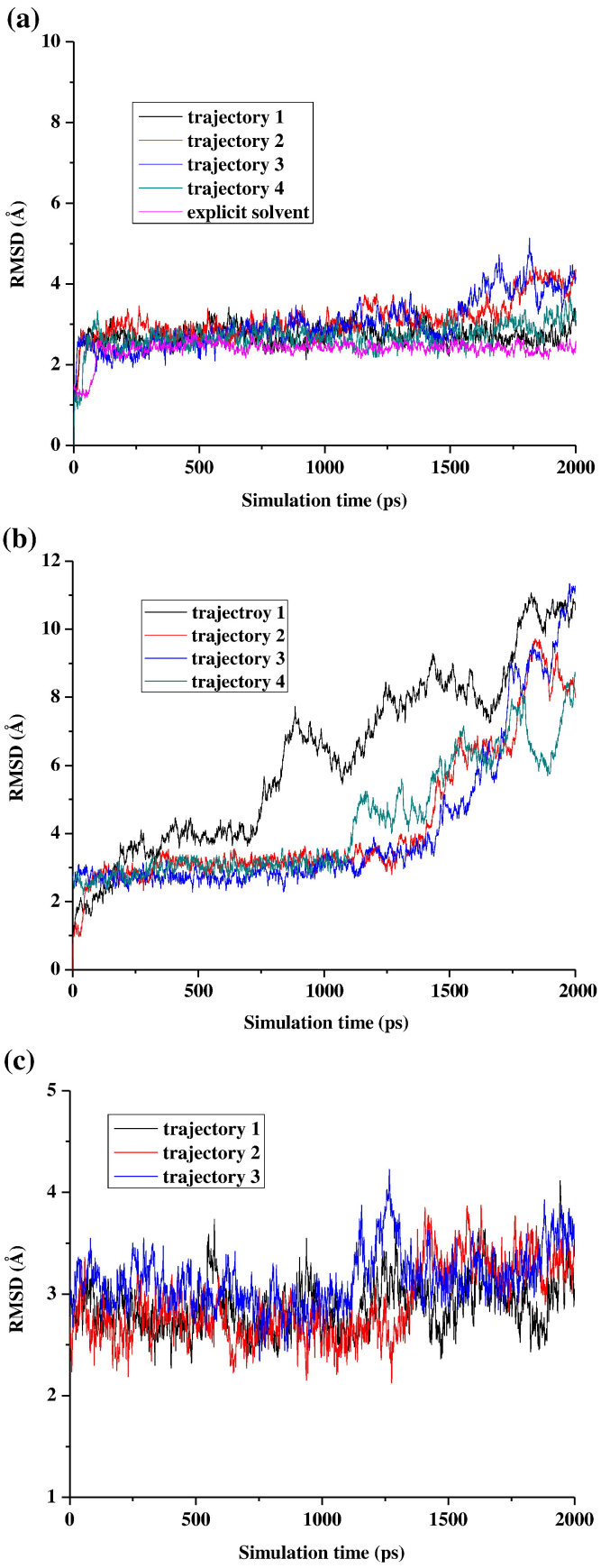

Fig. 5. Comparison of root mean square deviations (RMSD, Å) of MD trajectories from multiple dynamic simulations. a) GNNQQNY decamer alone b) GNNQQNY decamer with myricetin C) GNNQQNY decamer with kaempferol.

program from San Diego Supercomputer Center [42]. The myricetin molecule was placed ~5 Å away from the peptide oligomer along the β-sheet stacking direction.

2.3. MD simulations with implicit solvent model

The MD simulations and part of the analysis of the trajectories were conducted using the AMBER 10 suite of programs [43]. The peptide was modeled by the all-atom amber force field. The structure was minimized with steepest descent method for 500 iterations. After energy minimization, structures were equilibrated during 50 ps by gradually increasing the temperature from 0 to 300 K. It has been checked that, during the heating step, the potential energy reached a stable value. MD simulations were conducted using the generalized Born (GB) approximation at constant temperature (300 K) using the Langevin scheme. The list of nonbonded interactions was updated every 2 ps and 12 Å cutoff was used. SHAKE [44] was applied to constrain all bonds connecting hydrogen atoms to allow a time step of 2.0 fs. The water molecules from the crystal structure were removed and XLeAP (part of the AMBER package) was used to set up the calculations. After energy minimization, structures were equilibrated during 50 ps by gradually increasing the temperature from 0 to 300 K. The necessary checks have been made to ensure that the potential energy reached a stable value after this heating step. All the simulations were performed at constant temperature (300 K) for 2 ns. The molecular dynamic trajectories were saved every 500 steps (1 ps interval) for subsequent analysis. Hydrogen bond occupancies and structure RMSDs was calculated using PTRAJ module available within AMBER. A hydrogen bond is assigned if the distance between donor D and acceptor A is $\leq$3.5 Å and the angle D–H···A$\geq$120° [45]. A recent paper by Chapman et al. provides a detailed discussion of hydrogen bonding criteria [45]. In recent literature there is a tendency to use a lower cutoff for the angle based on the result in the paper above. For instance, the hydrogen bonds is defined by a distance between the donor and acceptor (d N–H···O) equal to or less than 3.0 Å and the angle NH···O bigger than 100° in Trbovic et al. [46]. The hydrogen bonds is defined by a distance between the donor and acceptor (d N–H···O) equal to or less than 2.5 Å and the angle N–H···O bigger than 120° in both Nussinov et al. [47,48]. The analysis employed by Nussinov et al. [47] specially are on fiber organization of octa-peptide amyloids a system similar to our model under investigation. The simulation results were visualized suing VMD 1.8.7 [49].

Implicit solvent simulation does not employ periodical boundary conditions. Therefore, a large separation between the molecules in the simulation is possible, contrary to a real situation with the finite concentrations. Similar to other implicit solvent MD simulation of the aggregation [50], we applied the harmonic constraint $k\ (r-r_0)^2/2$ between the center of mass of the ligand and the peptide molecules, when the distance r between them exceeded $r_0 = 20$ Å. The value of the force constant k used was 200 kcal/mol Å^2. The constraint does not affect the energy of the system at distances below 20 Å, but prevents the sampling of the large area of the configuration space that represents no appreciable interaction between the ligand and the aggregate. The constraint does not affect the energy of the system at distances below 20 Å, but prevents the sampling of the large area of the configuration space that represents no appreciable interaction between the ligand and the aggregate.

2.4. MD simulations with explicit solvation model

To test the performance of the implicit MD simulations of the GNNQQNY oligomer: was immersed in truncated octahedron box of TIP3P water molecules. The AMBER ff99SB force field was used to produce the force field parameters for the peptide. The simulation utilized the particle mesh Ewald (PME) method to treat long-range

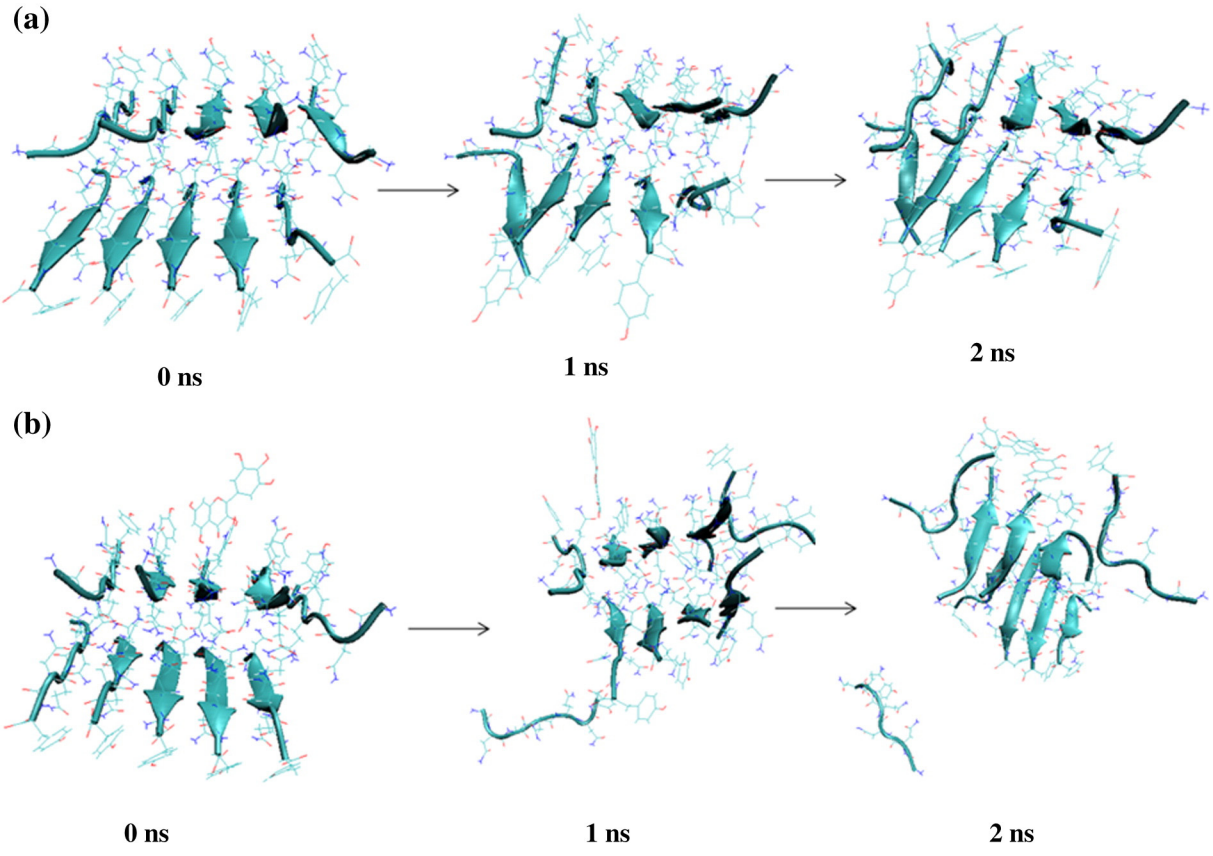

Fig. 6. Stable decamer of GNNQQNNY (a) during 2 ns MD simulations and destabilization of GNNQQNY fibrils with myricetin (b). The figure was generated using VMD.

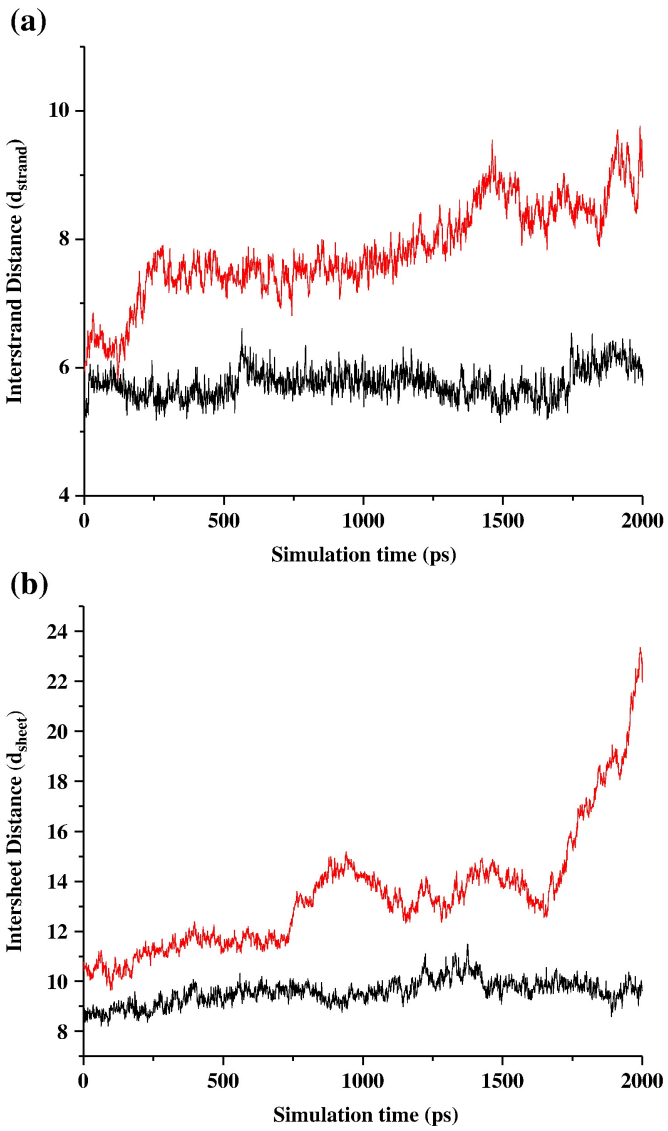

Fig. 7. Time evolution of the average interstrand and intersheet distance with respect to simulation time. (a) The average distance between two neighboring strands and b) the average distance between two neighboring sheets. Black line indicates GNNQQNY fibrils alone (trajectory 1) and red line indicates GNNQQNY fibril with myricetin (trajectory 1).

electrostatic interactions, with a cutoff of 12 Å and VdW cutoff of 12 Å. For the oligomer systems, in order to relax bond geometries, the potential energy of the system (peptides and water) was minimized by using the steepest descent method until convergence was reached. After energy minimization, structures were equilibrated during 50 ps by gradually increasing the temperature from 0 to 300 K. The necessary checks have been made to ensure that the potential energy reached a stable value after this heating step. The simulations were run with periodic boundary conditions. All the simulations were performed at constant temperature (300 K) and pressure (1 atom) for 2 ns. The molecular dynamic trajectories were saved every 500 steps (1 ps interval) for subsequent analysis.

3. Results and discussion

First we tested several AMBER force fields (ff96, ff99, ff99SB, and ff03) and implicit solvent models (igb1, igb2, igb5, and igb7) for their ability to keep the decamer of GNNQQNY aggregated. We performed constant temperature MD simulations, and the RMSD of both the explicit solvent and the implicit solvent trajectories, relative to the crystal structure, are plotted in Fig. 2(a–d). During the 2 ns of production run with explicit solvent, the decamer remained stable as evidenced by backbone RMSD of 2.0 Å. On the other hand, the results of the simulations using the implicit solvent models were varied. The details of the performance of force fields and solvent models results can be found in the supporting material. Based on our results and the literature data, we selected 99SB force field and igb5 solvation model to investigate the stability of the GNNQQNY oligomer in the presence of the myricetin (Figs. 3 and 4).

We performed multiple MD simulations for the decamer of GNNQQNY in implicit solvent with and without myricetin at room temperature changing the initial conditions by assigning random velocities according to Maxwell distribution to explore wider conformational space. The simulations were run for 10 ns. While the decamers with myricitin disaggregated within the first 1 ns, the decamer without small molecule starts to disaggregate only after 5 ns. For the first 5 ns the decamer was found to remain stable compared to the crystal structure as evidenced by RMSD, intersheet distance measurement and visual inspection of the trajectory using VMD. This

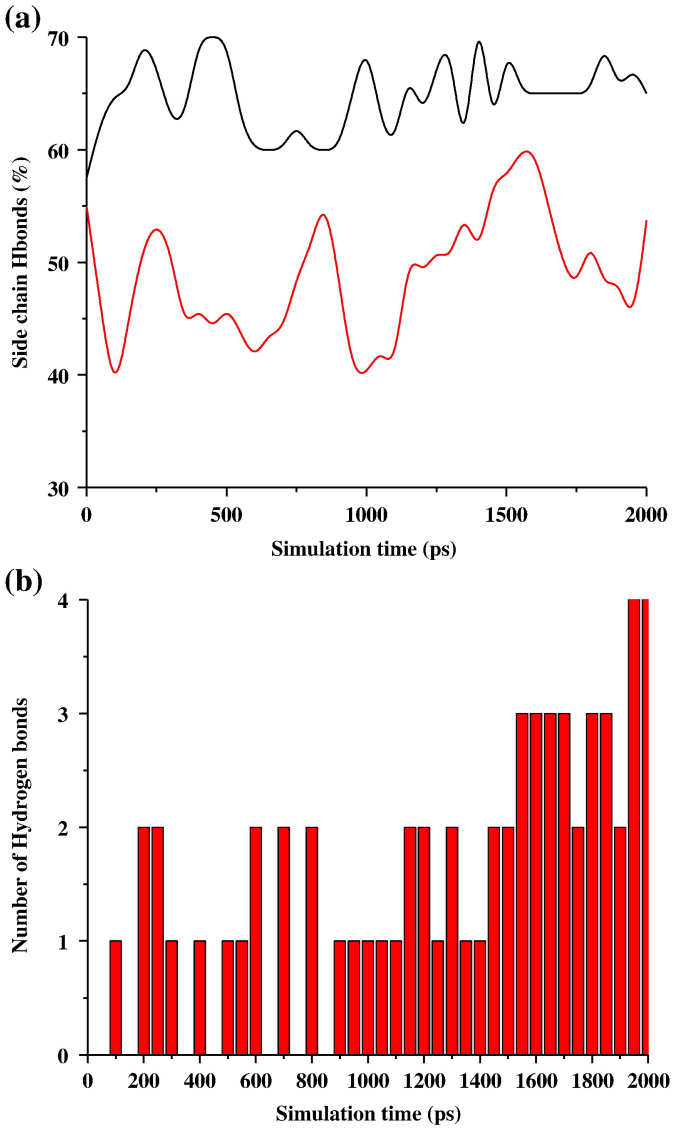

Fig. 8. a) Time evolution of the fraction of preserved hydrogen bonds between the two beta sheets, plotted as a percentage with respect to the starting point. Black line indicates GNNQQNY fibrils alone (trajectory 1) and red line indicates GNNQQNY fibril with myricetin (trajectory 1). b) Time evolution of the number of hydrogen bonds between myricetin and beta sheet layer.

faster disaggregation reflects aggregation inhibiting action of myricitin. Further, we compared the 2 ns trajectory of the decamer in explicit solvent to the first 2 ns trajectory of decamer in implicit solvent alone and with myricetin and kaempferol. While decamer alone in both implicit and explicit solvent maintained the structure close to the X-ray (RMSD<4 Å) in four out of five trajectories, all four trajectories describing the decamer interacting with myricetin resulted in dissociation (two strands in one case, and one strand separated from the aggregate in three other trajectories). Below we analyze two representative trajectories in details.

The plot of the RMSD for the oligomer with myricetin shown in Fig. 5 indicates the RMSD value increased rapidly to 4 Å within ~250 ps and it reaches ~12 Å within the 2 ns simulation time, indicating that the original structural organization of the oligomer was perturbed by the presence of myricetin. Ribbon/all atomic images of the selected snapshots from the simulation of the oligomer with and without myricetin are shown in Fig. 6 (a–b). While the β-strands in both sheets remain aggregated during the 2 ns simulation without myricetin (Fig. 6a), the simulation with myricetin leads to the complete dissociated of one of the β-strands within the first one nanosecond simulation time (Fig. 6b). Other deformations detected by the visual analysis include the increase curvature of the β-sheet, wrapping around the ligand, and increased separation between two β-sheets. This is consistent with previous simulation studies [25,27] found that inhibitors reduced the interstrand hydrogen bonding, although by a different mechanism.

Next, we quantify the perturbations brought about by myricitin and investigate the mechanism leading to oligomer dissociation. For this purpose we use global geometrical parameters, hydrogen bonding analysis, and potential energy plots. To examine the structural stability of GNNQQNY oligomers in the presence of the ligand and in its absence, we analyzed the interstrand and intersheet distances, introduced in refs. [12,48]. The interstrand distance (d_{strand}) was calculated by averaging the C_α distance between each residue in one β strand and its corresponding residues in the adjacent β strand within the same β strand layer. The intersheet (d_{sheet}) distance is calculated by averaging the distance between each strand in one sheet and its corresponding strand in the adjacent sheet [12,48]. The results of the interstrand and intersheet results are discussed below.

The initial interstrand distance, compared to the experimental value of 4.76 Å may measure the structural stability of the oligomer in the presence and absence of myricetin. Fig. 7a shows that the d_{strand} remains within the range of 5 to 7 Å without the polyphenol indicating the two sheets maintain their original organization. However in the presence of myricetin it increases up to 14 Å, indicating that the original structure becomes unstable. Another geometrical parameter is intersheet distance. Fig. 7b shows that without myricetin the two β-sheets of the GNNQQNY oligomer remain within the range of 9–10 Å, close to the experimental value of 8.70 Å [2,8]. In the presence of myricetin the intersheet distance is increased to the range of 10–24 Å indicating that two β-sheets are moving away from each other as shown in Fig. 7b.

Hydrogen bond analysis can serve as another method to characterize structural perturbations. On one hand, H-bonds are necessary to form the β-sheet, the main conformational pattern of amyloid fibrils [48]. On the other hand, the importance of H-bonding side chain interactions on the stabilization of β rich structures has been observed in several studies [51–53]. Akaishi et al. [54] identified that the important trends in the structure/activity relationship for polyphenols are directly related to the hydrogen bonding. In the study of flavonoid amyloid beta aggregation inhibitors they have found that simultaneous presence of 3′,4′-dihydroxyl groups, but not the 3- or 7-hydroxyl groups is essential for the inhibitor effect. Kaempferol without the 3′-hydroxyl group shows less inhibitory activity compared to myricetin which has both the 3′- and 4′-hydroxyl groups. They concluded that increasing the number of hydroxyl groups on ring B potentiates the inhibitor effect. Myricetin binds to the peptide backbone through its hydroxyl groups trapping critical hydrogen bonds in the peptide aggregate.

In order to reveal the mechanism by which the specific chemical structure is related to disaggregation, we report the analysis of H-bonding between two β-sheets (Fig. 8a) and between myricetin and the peptide (Fig. 8b). As one can see, in the absence of myricetin

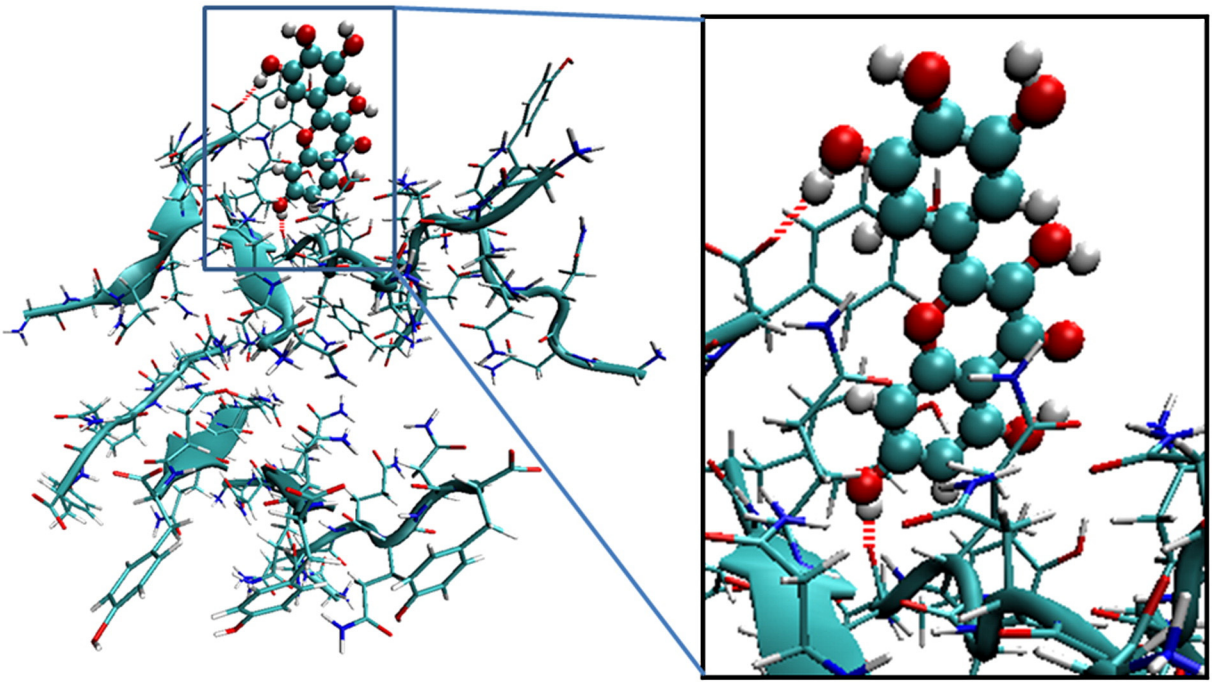

Fig. 9. Complete (left) and enlarged (right) 1.8 ns snapshot from one of the trajectories shows that myricetin forms H-bonds with the surface of the β-sheet, weakening the interstrand hydrogen bonds, wrapping the β-sheet around the myricitin. This breaks backbone H-bonding and separates the layers from each other and one the β-strands from the outer layer.

the number of hydrogen bonds between the two beta sheets is greater than in its presence. The result also shows that the number of H-bonds between the beta sheets decreased rapidly in the presence of the myricetin, compared to the free decamer (Fig. 8a). While the aggregate without myricetin is able to maintain close to 60% of the original hydrogen bonds between the sheets, the same aggregate in the presence of myricetin retains on only c.a. 45% of the original hydrogen bonds. The reasons for this loss of H-bonding become clear after one examines Fig. 8b. From this figure one can see that the myricetin is forming hydrogen bonds with both peptide backbone NH group and side chain NH groups, weakening the backbone to backbone H-bonds between the strands in the beta sheet closer to the inhibitor molecule. In addition, side chain to side chain H-bonding is also lost, thus destabilizing the steric zipper aggregation between the two beta sheets. Meersman et al. [55] have previously reported that both side chain interactions and backbone H-bonds lend considerable stability to amyloid fibrils against dissociation.

Thus, our simulations show that myricetin forms H-bonds with the surface of the β-sheet, weakening the interstrand hydrogen bonds, wrapping the β-sheet and disaggregating the outer layer. The detailed analysis shows that both backbone to backbone and side chain to side chain hydrogen bonds are lost, and the β-sheets are moving away from each other. This leads to the loss of the backbone H-bonding and eventual separation of one the β-strands in from the outer layer. One can see these effects on the 1.8 ns snapshot from one of the trajectories (Fig. 9). As follows from the figure, forming two H-bonds with the surface of the peptide is essential for aggregation inhibiting properties of myricetin. Kaempferol, on the other hand, is missing 3′- and 5′-hydroxyl and is unable to form similar H-bonded complex. This explains its weaker inhibiting properties.

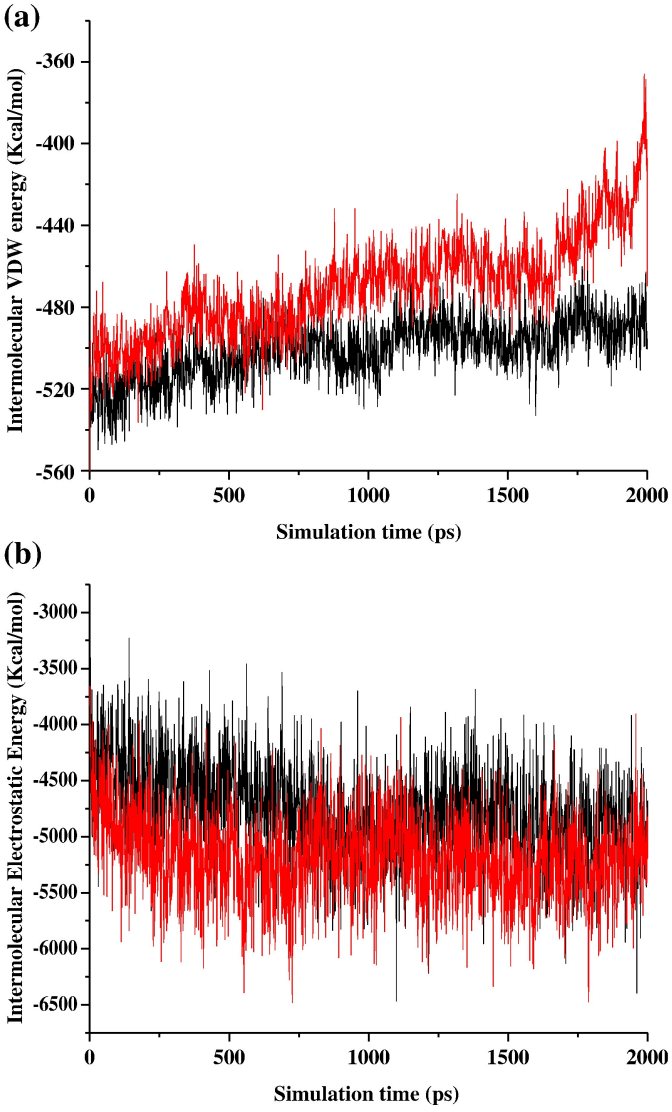

Fig. 10. Plots of the different components to the intermolecular interaction energy of the aggregate with and without myricetin: (a) van der Waals and (b) electrostatic energy. Black line indicates GNNQQNY decamer alone and red line indicates GNNQQNY decamer with myricetin.

Let us now turn to the energetic aspects of the ligand effect. The *vdw* forces were recently proposed a quantitative measure of the shape complementarily among side chains between β-sheets [56]. We report the intermolecular electrostatic and van der Waals (*vdw*) energy of the oligomer with and without myricetin in Fig. 10. One can see that the vdw energy of oligomer alone is lower than the case of oligomer with myricetin system during the simulation times (Fig. 10a). Intermolecular vdw interaction for the oligomer with myricetin becomes less attractive by c.a. 30 kcal/mol compared to that of the oligomer without myricetin (*vdw* energy is increased to −470 kcal/mol from −501 kcal/mol on average). This means that myricetin molecule has pronounced destabilization effect in bilayer pattern by reducing the intermolecular vdw interaction, in agreement with previous observations [56]. In contrast, the intermolecular electrostatic energies during MD simulations are virtually indistinguishable between the oligomer with and without myricetin (Fig. 10b).

We also investigated the sensitivity of the results to the nature of the aggregate inhibitor. To that end we repeated the simulations in the presence of kaempferol, a ligand known to be considerably less effective in destabilizing the aggregates. The plot of the RMSD for the decamer with kaempferol shown in Fig. 5. One can see that RMSD value remained within 4 Å during the 2 ns simulation time in all 3 trajectories considered. This indicates that the original structural organization of the aggregates was not perturbed by the presence of kaempferol.

4. Conclusions

Comparison of the MD simulations of the decamer of GNNQQNY and myricetin/decamer GNNQQNY complex demonstrates that myricretin disturbs the stability of decamer of GNNQQNY. The simulations show myricetin interacts with the β-sheet due to polar interactions with side chains of the peptide weakening the interstrand hydrogen bonds, wrapping the β sheet and disaggregating the outer layer. The detailed analysis show that both side chain to side chain hydrogen bonds are lost, and the β-sheets are moving away from each other. This leads to the loss of the backbone H-bonding and eventual separation of one the β-strands in from the outer layer. The MD simulation provides the understanding of the mechanism by which the small molecules destabilizes the ordered oligomer. Based on our study we conclude that computational methodology can make a contribution toward understanding the destabilizing effect of the natural polyphenolic compounds on amyloid aggregation and thus could be used in the design of new non-peptide anti-amyloidogenic drug molecules.

Acknowledgments

This work was supported in part by the National Science Foundation (CCF/CHE 0832622). The authors are thankful to UCF Institute for Simulations and Training (IST) HPC Stokes facility, UCF I2Lab, and U.S. Department of Energy National Energy Research Scientific Computing Center (DOE NERSC) for the generous donation of the computer time.

Appendix A. Supplementary data

Supplementary data associated with this article can be found, in the online version, at doi:10.1016/j.bpc.2010.03.003.

References

[1] A.J. Howie, D.B. Brewer, D. Howell, A.P. Jones, Laboratory Investigation 88 (2008) 232–242, doi:10.1038/labinvest.3700714.
[2] M.R. Sawaya, S. Sambashivan, R. Nelson, M.I. Ivanova, S.A. Sievers, M.I. Apostol, M.J. Thompson, M. Balbirnie, J.J.W. Wiltzius, H.T. McFarlane, A.O. Madsen, C. Riekel, D. Eisenberg, Nature 447 (2007) 453–457, doi:10.1038/nature05695.
[3] C.M. Dobson, Trends Biochemical Sciences 24 (1999) 329–332.
[4] Y. Porat, A. Abramowitz, E. Gazit, Chemical Biology & Drug Design 67 (2006) 27–37, doi:10.1111/j.1747-0285.2005.00318.x.
[5] L.L. Blazer, R.R. Neubig, Neuropsychopharmacology 34 (2009) 126–141, doi:10.1038/npp. 2008.151.
[6] S.N. Haydar, H.E.D. Yun, R.G.W. Staal, W.D. Hirst, Annual Reports in Medicinal Chemistry, vol. 44, Elsevier Academic Press Inc, San Diego, 2009, pp. 51–69.
[7] J.D. Sipe, A.S. Cohen, Journal of Structural Biology 130 (2000) 88–98.
[8] R. Nelson, M.R. Sawaya, M. Balbirnie, A.O. Madsen, C. Riekel, R. Grothe, D. Eisenberg, Nature 435 (2005) 773–778, doi:10.1038/nature03680.
[9] L. Esposito, C. Pedone, L. Vitagliano, Proceedings of the National Academy of Sciences of the United States of America 103 (2006) 11533–11538, doi:10.1073/pnas.0602345103.
[10] M. Meli, G. Morra, G. Colombo, Biophysical Journal 94 (2008) 4414–4426, doi:10.1529/biophysj.107.121061.
[11] Z.Q. Zhang, H. Chen, H.J. Bai, L.H. Lai, Biophysical Journal 93 (2007) 1484–1492, doi:10.1529/biophysj.106.100537.
[12] J. Zheng, B.Y. Ma, C.J. Tsai, R. Nussinov, Biophysical Journal 91 (2006) 824–833, doi:10.1529/biophysj.106.083246.
[13] J. Gsponer, U. Haberthur, A. Caflisch, Proceedings of the National Academy of Sciences of the United States of America 100 (2003) 5154–5159, doi:10.1073/pnas.0835307100.
[14] J. Wang, C.H. Tan, H.F. Chen, R. Luo, Biophysical Journal 95 (2008) 5037–5047, doi:10.1529/biophysj.108.131672.
[15] P. Frid, S.V. Anisimov, N. Popovic, Brain Research Reviews 53 (2007) 135–160, doi:10.1016/j.brainresrev.2006.08.001.
[16] C.A. Hawkes, V. Ng, J. McLaurin, Drug Development Research 70 (2009) 111–124, doi:10.1002/ddr.20290.
[17] R.W. Hepler, K.M. Grimm, D.D. Nahas, R. Breese, E.C. Dodson, P. Acton, P.M. Keller, M. Yeager, H. Wang, P. Shughrue, G. Kinney, J.G. Joyce, Biochemistry 45 (2006) 15157–15167, doi:10.1021/bi061850f.
[18] S. Lesne, M.T. Koh, L. Kotilinek, R. Kayed, C.G. Glabe, A. Yang, M. Gallagher, K.H. Ashe, Nature 440 (2006) 352–357, doi:10.1038/nature04533.
[19] M. Bucciantini, E. Giannoni, F. Chiti, F. Baroni, L. Formigli, J.S. Zurdo, N. Taddei, G. Ramponi, C.M. Dobson, M. Stefani, Nature 416 (2002) 507–511.
[20] M. Bucciantini, G. Calloni, F. Chiti, L. Formigli, D. Nosi, C.M. Dobson, M. Stefani, Journal of Biological Chemistry 279 (2004) 31374–31382, doi:10.1074/jbc.M400348200.
[21] J. Hardy, D.J. Selkoe, Science 297 (2002) 353–356.
[22] M. Hirohata, K. Hasegawa, S. Tsutsumi-Yasuhara, Y. Ohhashi, T. Ookoshi, K. Ono, M. Yamada, H. Naiki, Biochemistry 46 (2007) 1888–1899, doi:10.1021/bi061540x.
[23] K. Ono, Y. Yoshiike, A. Takashima, K. Hasegawa, H. Naiki, M. Yamada, Journal of Neurochemistry 87 (2003) 172–181, doi:10.1046/j.1471-4159.2003.01976.x.
[24] Y.S. Kim, J.H. Lee, J. Ryu, D.J. Kim, Current Pharmaceutical Design 15 (2009) 637–658.
[25] M. Convertino, R. Pellarin, M. Catto, A. Carotti, A. Caflisch, Protein Science 18 (2009) 792–800, doi:10.1002/pro.87.
[26] C. Wu, Z.X. Wang, H.X. Lei, W. Zhang, Y. Duan, Journal of the American Chemical Society 129 (2007) 1225–1232, doi:10.1021/ja0662772.
[27] F.F. Liu, L. Ji, X.Y. Dong, Y. Sun, Journal of Physical Chemistry B 113 (2009) 11320–11329, doi:10.1021/jp905580j.
[28] B. Mothana, S. Roy, A. Rauk, Arkivoc (2009) 116–134.
[29] V. Tsui, D.A. Case, Biopolymers 56 (2000) 275–291.
[30] M. Feig, C.L. Brooks, Current Opinion in Structural Biology 14 (2004) 217–224, doi:10.1016/j.sbi.2004.03.009.
[31] J. Wang, C.H. Tan, Y.H. Tan, Q. Lu, R. Luo, Communications in Computational Physics 3 (2008) 1010–1031.
[32] J. Chocholousova, M. Feig, Journal of Physical Chemistry B 110 (2006) 17240–17251, doi:10.1021/jp0627675.
[33] L. Peter, Cummins AABaJEG, in: H.D.W. Partrick Bultinck, Wilfried Langeneaeker, Jan P. Tollenaere (Eds.), Solvent model Marcel Dekker, Inc, New York, 2004.
[34] J.H. Chen, C.L. Brooks, J. Khandogin, Current Opinion in Structural Biology 18 (2008) 140–148, doi:10.1016/j.sbi.2008.01.003.
[35] T.Z. Lwin, R. Luo, Protein Science 15 (2006) 2642–2655, doi:10.1110/ps.062438006.
[36] A.D. Mackerell, Journal of Computational Chemistry 25 (2004) 1584–1604, doi:10.1002/jcc.20082.
[37] M.S. Shell, R. Ritterson, K.A. Dill, Journal of Physical Chemistry B 112 (2008) 6878–6886, doi:10.1021/jp800282x.
[38] W.D. Cornell, P. Cieplak, C.I. Bayly, I.R. Gould, K.M. Merz, D.M. Ferguson, D.C. Spellmeyer, T. Fox, J.W. Caldwell, P.A. Kollman, Journal of the American Chemical Society 117 (1995) 5179–5197.
[39] R. Kayed, E. Head, J.L. Thompson, T.M. McIntire, S.C. Milton, C.W. Cotman, C.G. Glabe, Science 300 (2003) 486–489.
[40] M.J.T.G.W. Frisch, H.B. Schlegel, G.E. Scuseria, M.A. Robb, J.R. Cheeseman, J.A. Montgomery Jr., T. Vreven, K.N. Kudin, J.C. Burant, J.M. Millam, S.S. Iyengar, J. Tomasi, V. Barone, B. Mennucci, M. Cossi, G. Scalmani, N. Rega, G.A. Petersson, H. Nakatsuji, M. Hada, M. Ehara, K. Toyota, R. Fukuda, J. Hasegawa, M. Ishida, T. Nakajima, Y. Honda, O. Kitao, H. Nakai, M. Klene, X. Li, J.E. Knox, H.P. Hratchian, J.B. Cross, V. Bakken, C. Adamo, J. Jaramillo, R. Gomperts, R.E. Stratmann, O. Yazyev, A.J. Austin, R. Cammi, C. Pomelli, J.W. Ochterski, P.Y. Ayala, K. Morokuma, G.A. Voth, P. Salvador, J.J. Dannenberg, V.G. Zakrzewski, S. Dapprich, A.D. Daniels, M.C. Strain, O. Farkas, D.K. Malick, A.D. Rabuck, K. Raghavachari, J.B. Foresman, J.V. Ortiz, Q. Cui, A.G. Baboul, S. Clifford, J. Cioslowski, B.B. Stefanov, G. Liu, A. Liashenko, P. Piskorz, I. Komaromi, R.L. Martin, D.J. Fox, T. Keith, M.A. Al-Laham, C.Y. Peng, A. Nanayakkara, M. Challacombe, P.M.W. Gill, B. Johnson, W. Chen, M.W. Wong, C. Gonzalez, J.A. Pople, Gaussian, Inc, Wallingford CT, 2004.
[41] http://www.doe-mbi.ucla.edu/sawaya/chime/xtalpept (2009).
[42] http://sirius.sdsc.edu (2009).
[43] D.A. Case TAD, T.E. Cheatham III, C.L. Simmerling, J. Wang, R.E. Duke, R. Luo, M. Crowley, Ross C. Walker, W. Zhang, K.M. Merz, B. Wang, S. Hayik, A. Roitberg, G. Seabra, I. Kolossváry, K.F. Wong, F. Paesani, J. Vanicek, X. Wu, S.R. Brozell, T. Steinbrecher, H. Gohlke, L. Yang, C. Tan, J. Mongan, V. Hornak, G. Cui, D.H. Mathews, M.G. Seetin, C. Sagui, V. Babin, P.A. Kollman, University of California, San Francisco, 2008.
[44] J.P. Ryckaert, G. Ciccotti, H.J.C. Berendsen, Journal of Computational Physics 23 (1977) 327–341.
[45] F. Fabiola, R. Bertram, A. Korostelev, M.S. Chapman, Protein Science 11 (2002) 1415–1423, doi:10.1110/ps.4890102.
[46] N. Trbovic, J.H. Cho, R. Abel, R.A. Friesner, M. Rance, A.G. Palmer, Journal of the American Chemical Society 131 (2009) 615–622, doi:10.1021/ja806475k.
[47] D. Zanuy, R. Nussinov, Journal of Molecular Biology 329 (2003) 565–584, doi:10.1016/s0022-2836(03)00491-1.
[48] D. Zanuy, Y. Porat, E. Gazit, R. Nussinov, Structure 12 (2004) 439–455, doi:10.1016/j.str.2004.02.002.
[49] W. Humphrey, A. Dalke, K. Schulten, Journal of Molecular Graphics 14 (1996) 33–38.
[50] P. Anand, F.S. Nandel, U.H.E. Hansmann, Journal of Chemical Physics 129 (7) (2008) 195102, doi:10.1063/1.3021062.
[51] G. Colombo, I. Daidone, E. Gazit, A. Amadei, A. Di Nola, Proteins-Structure Function and Bioinformatics 59 (2005) 519–527, doi:10.1002/prot.20426.
[52] M.L. de la Paz, E. Lacroix, M. Ramirez-Alvarado, L. Serrano, Journal of Molecular Biology 312 (2001) 229–246.
[53] G. Colombo, G.M.S. De Mori, D. Roccatano, Protein Science 12 (2003) 538–550, doi:10.1110/ps.0227203.
[54] T. Akaishi, T. Morimoto, M. Shibao, S. Watanabe, K. Sakai-Kato, N. Utsunomiya-Tate, K. Abe, Neuroscience Letters 444 (2008) 280–285, doi:10.1016/j.neulet.2008.08.052.
[55] F. Meersman, C.M. Dobson, BBA-Proteins Proteomics 1764 (2006) 452–460, doi:10.1016/j.bbapap. 2005.10.021.
[56] J. Park, B. Kahng, W. Hwang, Plos Computational Biology 5 (17) (2009) e1000492, doi:10.1371/journal.pcbi.1000492.